Hydrogen Evolution Reaction | Hot Paper

DOI: 10.1002/anie.201409524

Enhanced Electron Penetration through an Ultrathin Graphene Layer for Highly Efficient Catalysis of the Hydrogen Evolution Reaction**

Jiao Deng, Pengju Ren, Dehui Deng, and Xinhe Bao**

Abstract: *Major challenges encountered when trying to replace precious-metal-based electrocatalysts of the hydrogen evolution reaction (HER) in acidic media are related to the low efficiency and stability of non-precious-metal compounds. Therefore, new concepts and strategies have to be devised to develop electrocatalysts that are based on earth-abundant materials. Herein, we report a hierarchical architecture that consists of ultrathin graphene shells (only 1–3 layers) that encapsulate a uniform CoNi nanoalloy to enhance its HER performance in acidic media. The optimized catalyst exhibits high stability and activity with an onset overpotential of almost zero versus the reversible hydrogen electrode (RHE) and an overpotential of only 142 mV at 10 mA cm^{-2}, which is quite close to that of commercial 40 % Pt/C catalysts. Density functional theory (DFT) calculations indicate that the ultrathin graphene shells strongly promote electron penetration from the CoNi nanoalloy to the graphene surface. With nitrogen dopants, they synergistically increase the electron density on the graphene surface, which results in superior HER activity on the graphene shells.*

Hydrogen, a renewable and clean fuel, is considered as a potential energy carrier for future energy infrastructure.[1,2] The electrocatalytic splitting of water by the hydrogen evolution reaction (HER) is an important process with high energy conversion efficiency for hydrogen production.[3] Currently, the state-of-the-art catalysts are based on precious metals, such as platinum,[4–6] but their limited Earth resource and high cost hinder the commercial application of this technology. Compounds such as MoS_2,[7–12] Mo_2C,[13] MoB,[13] MoP,[14] $MoSe_2$,[15] WS_2,[16] and 3d transition metals (TMs),[17–19] have been studied as potential substitutes for Pt-based catalysts for a long time. Recently, 3d TMs such as Fe, Co, Ni, and their derivatives have received increasing attention as potential replacements of Pt-based catalysts owing to their earth abundance and low cost,[20–22] but these metals readily suffer from corrosion in acidic solid polymer electrolytes.

To this end, we have previously proposed a strategy to encapsulate 3d TMs into carbon nanotubes, which can efficiently prevent the corrosion of 3d TMs in acidic medium and simultaneously promote the catalytic reaction on the carbon surface owing to electron penetration from the encapsulated 3d TMs.[23] This strategy represents a new concept for maintaining the high activity and stability of non-precious metals in acidic medium and has recently been further applied in a variety of catalytic systems, for example, for the oxygen reduction reaction (ORR),[23–26] the HER under acidic conditions,[27,28] the triiodide reduction reaction in dye-sensitized solar cells (DSSCs),[29] and the heterogeneously catalyzed oxidation and reduction reactions.[30,31] However, the carbon shells previously used for these catalysts are too thick and usually consist of multilayer graphitic carbon or composites thereof, which may significantly reduce the catalytic activity as the electronic structure of the outermost carbon layer is only modulated by the electron transferred from the encapsulated metal core when the shell consist of no more than three to four carbon layers.[32,33] Therefore, the synthesis of carbon-encapsulated 3d TM catalysts with a controllable number of graphene layers, especially of catalysts with less than three layers of graphene, will be important for the development of 3d TM catalysts with superior HER activity. Herein, we report a bottom-up method for the preparation of ultrathin graphene spheres with only one to three graphene layers that encapsulate CoNi nanoalloy (CoNi@NC) electrocatalysts by using Co^{2+}, Ni^{2+}, and ethylenediaminetetraacetate anions ($EDTA^{4-}$) as precursors (see the Supporting Information, Figure S1 for details).

Scanning electron microscopy (SEM; Figure 1b, Figure S3) and transmission electron microscopy (TEM; Figure 1c, Figure S4) images show that the CoNi@NC samples consist of uniform nanospheres, forming lamellar superstructures on the micrometer scale (Figure 1a). Further high-resolution (HR) TEM analysis indicates that the nanospheres consist of metal nanoparticles (NPs) that are completely coated by graphene shells (Figure 1d, Figure S4–7). The metal NPs have a uniform size of generally 4–7 nm (see the statistical analysis in Figure 1c, inset) with a *d*-spacing of 0.215 nm, which corresponds to the (111) plane of the CoNi alloy (Figure 1e). According to the statistical analysis by

[*] J. Deng,[+] P. Ren,[+] D. Deng, X. Bao
State Key Laboratory of Catalysis
Dalian Institute of Chemical Physics
Chinese Academy of Sciences
Zhongshan Road 457, Dalian, 116023 (China)
E-mail: dhdeng@dicp.ac.cn
xhbao@dicp.ac.cn

[+] These authors contributed equally to this work.

[**] We gratefully acknowledge financial support from the National Natural Science Foundation of China (21321002, 21033009, and 21303191) and the Strategic Priority Research Program of the Chinese Academy of Sciences (XDA09030100). We thank staff at the BL14W1 beamline of the Shanghai Synchrotron Radiation Facilities (SSRF) for assistance with the XANES measurements. We thank Prof. Ze Zhang, Prof. Yong Wang, and Wentao Yuan for help with HAADF–STEM characterization, and Prof. Fan Yang and Dr. Jianping Xiao for fruitful discussions and manuscript proofreading.

Supporting information for this article is available on the WWW under http://dx.doi.org/10.1002/anie.201409524.

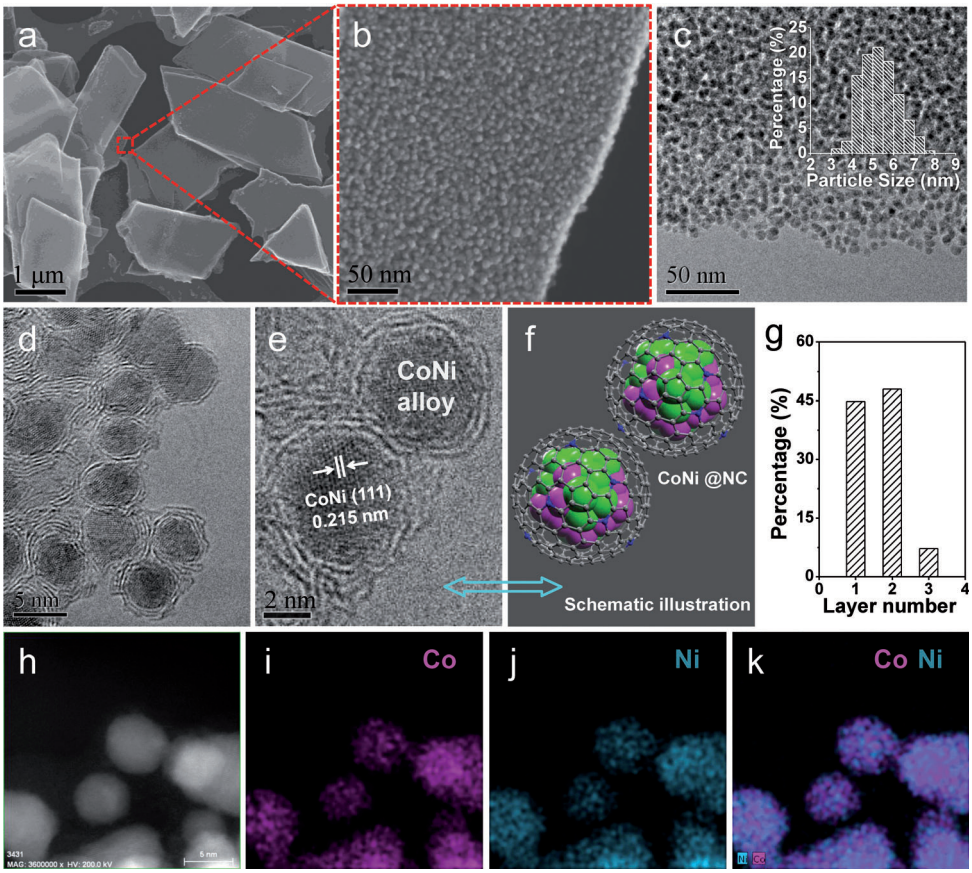

Figure 1. a, b) SEM images of CoNi@NC. The magnified image in (b) clearly reveals the uniformly sized nanospheres. c) TEM image of CoNi@NC showing a similar structure as (b). Inset: particle size distribution of the metal nanoparticles. d, e) HRTEM images of CoNi@NC, showing the graphene shells and encapsulated metal nanoparticles. Inset (e): crystal (111) plane of the CoNi alloy. f) Schematic illustration of the CoNi@NC structure shown in (e). g) Statistical analysis of the number of layers in the graphene shells encapsulating the metal nanoparticles in CoNi@NC. h–k) HAADF–STEM image and corresponding EDX maps of CoNi@NC for Co (i), Ni (j), and combined image (k).

HRTEM (Figure 1 g), the graphene shells on the CoNi NPs are very thin (only 1–3 layers), and most of the graphene shells (> 90 %) consist of only one to two layers. A high-angle annular dark-field scanning transmission electron microscopy (HAADF–STEM) image with sub-Ångström resolution further confirmed that uniform metal NPs had been formed (Figure 1 h), and the corresponding energy-dispersive X-ray (EDX) maps showed that the Co and Ni atoms were distributed homogeneously over all NPs (Figure 1 i–k), further confirming the alloy structure of CoNi.

Synchrotron-based X-ray absorption near-edge structure (XANES) analysis, X-ray photoelectron spectroscopy (XPS), and X-ray diffraction (XRD) were used to investigate the electronic and structural properties of CoNi@NC. The XANES spectra of the Co K-edge and the Ni K-edge indicated that Co and Ni are in a metallic state in all CoNi@NC samples independent of the annealing temperature (Figure 2 a,b), which is consistent with the Co 2p and Ni 2p XPS spectral analysis (Figure 2 c). The XRD spectra showed that except for the graphitic carbon shell and the CoNi alloy, no other phases are present in the CoNi@NC samples (Figure 2 d). Furthermore, the broad peaks of the CoNi alloy in the XRD pattern confirm that the metals are present as nanosized particles, which is consistent with the TEM statistical analysis (Figure 1 c). The very weak and broad C (002) peaks also confirm that ultrathin graphene shells have been formed, which is in agreement with the statistical analysis of the number of layers by HRTEM (Figure 1 g). These results indicate that uniform CoNi nanoalloys have been completely encapsulated in ultrathin graphene shells.

A typical three-electrode setup was adopted to evaluate the HER performance of the CoNi@NC samples in H_2SO_4 electrolyte (0.1 M). As shown in Figure 3 a, a blank glassy carbon (GC) electrode, the EDTA–CoNi complex, and pristine carbon nanotubes (CNTs) showed negligible or poor HER activities. In contrast, all CoNi@NC catalysts prepared at different annealing temperatures exhibited a higher HER activity. The CoNi@NC sample prepared at 475 °C gave the highest activity, with an onset overpotential of only approximately 30 mV and an overpotential of 224 mV at a current density of 10 mA cm^{-2}. Furthermore, the CoNi@NC samples prepared at different temperatures exhibited a fairly stable performance within accelerated degradation measurements for 1000 cyclic voltammetry (CV) cycles (Figure 3 c) or during a galvanostatic measurement at a current density of 20 mA cm^{-2} for 24 hours (Figure S10). The structures of the carbon shells encapsulating the metal nanoparticles were well maintained after the HER durability measurements, as confirmed by HRTEM (Figure S11) and Raman analysis (Figure S12).

According to previous studies, the introduction of nitrogen into carbon materials or metal/carbon composites may have an important effect on the catalytic activity.[23,29,34] Raman analysis firstly excluded the influence of graphitization on the HER activity (Figure S9). Further chemical composition analysis showed that the nitrogen concentration (N/C) decreased gradually with an increase in annealing temperature (Figure 3 b, Table S1), and the corresponding HER activity increased with an increase in nitrogen content. However, the CoNi@NC sample prepared at 425 °C showed

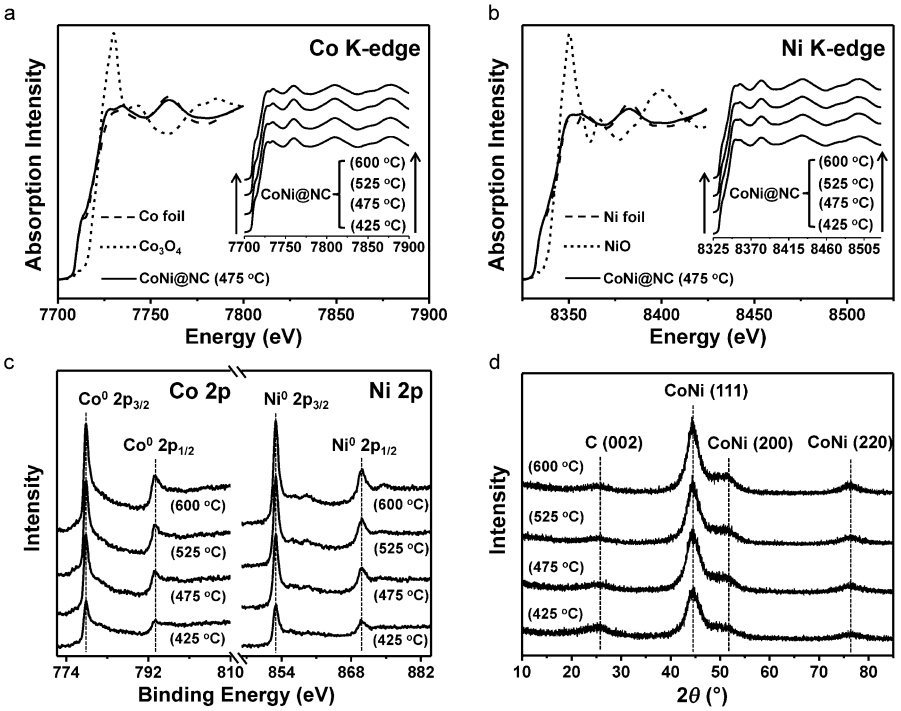

Figure 2. a, b) Co K-edge and Ni K-edge XANES spectra of CoNi@NC samples. Insets: Corresponding XANES spectra of CoNi@NC samples prepared at different annealing temperatures. c) Co 2p and Ni 2p XPS spectra of these CoNi@NC samples. d) XRD patterns of these CoNi@NC samples.

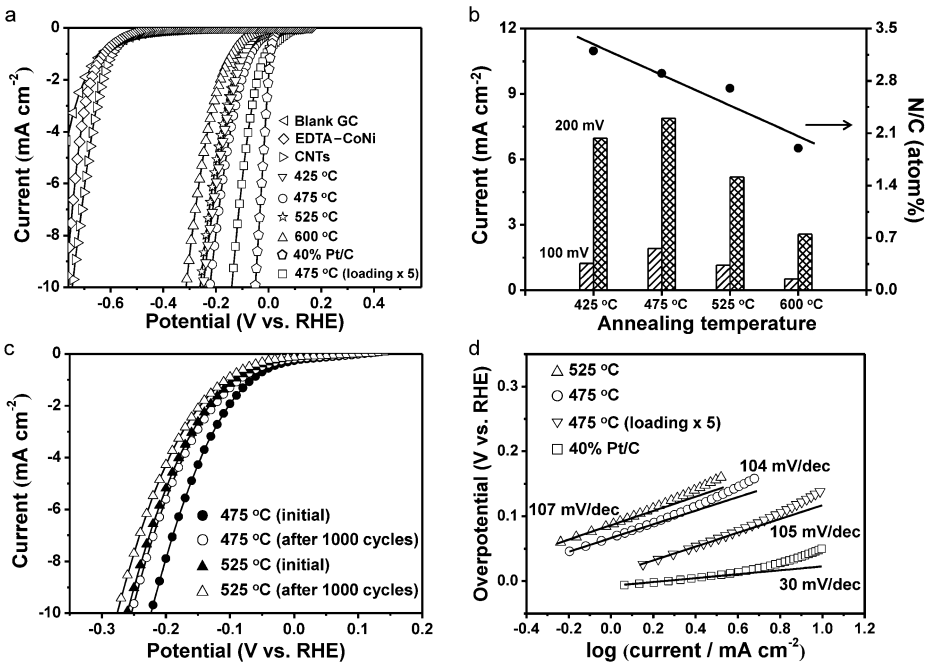

Figure 3. a) HER polarization curves for CoNi@NC samples prepared at different temperatures as well as for a CoNi@NC sample prepared at 475 °C with a catalyst mass loading of five equivalents on GC electrode compared to those of EDTA–CoNi, CNTs, 40% Pt/C, and a blank GC electrode. b) Current densities at overpotentials of 100 mV and 200 mV and the nitrogen concentration (N/C) as a function of the annealing temperature employed to synthesize the CoNi@NC sample. c) Durability measurements with CoNi@NC prepared at 475 °C and 525 °C. Polarization curves were recorded before the first and after 1000 CV sweeps between −142 mV and +108 mV (vs. RHE) at 100 mVs^{-1}. d) Tafel plots for CoNi@NC samples prepared at 475 °C and 525 °C as well as for 40% Pt/C and the CoNi@NC sample prepared at 475 °C with a catalyst mass loading of five equivalents on GC electrode.

a slightly lower activity than that prepared at 475 °C even though the former had a higher nitrogen content. We hypothesize that the distinctively smaller metal content of the sample prepared at 425 °C compared with the sample prepared at 475 °C (Table S1) may offset the contribution of the nitrogen dopants to the catalytic activity, leading to a higher HER activity for the sample prepared at 475 °C.

When the mass loading of catalyst on GC electrode was further increased to 5 wt equivalents, the HER activity of the CoNi@NC catalyst obtained at 475 °C was further enhanced with an onset overpotential of almost zero (ca. 0 mV vs. the reversible hydrogen electrode (RHE)) and an overpotential of only 142 mV at a current density of 10 mA cm^{-2} (Figure 3 a). To the best of our knowledge, this compound is the most efficient carbon-based HER electrocatalyst in acidic medium reported thus far (see Table S2).

Tafel slopes can be used to reveal the inherent reaction processes of the HER.[5,35] For the 40% Pt/C electrocatalyst used in this study, a value of 30 mV dec^{-1} was determined, which is consistent with previously reported results.[5] In contrast, values of 107 mV dec^{-1} and 104 mV dec^{-1} were obtained for the CoNi@NC samples prepared at 525 °C and 475 °C, respectively. The similar values for CoNi@NC prepared at 475 °C with different mass loadings shows that the Tafel slopes are almost independent of the catalyst mass loading (Figure 3 d). These results indicate that the HER catalyzed by these CoNi@NC samples is likely to occur by a Volmer–Heyrovsky mechanism.[5,27,35]

Density functional theory (DFT) calculations were carried out to gain further insights into the nature of this catalytic process. The processes that occur during the HER can be summarized in a three-state diagram, consisting of an initial H^+ state, an intermediate H* state and 1/2 H_2 as the

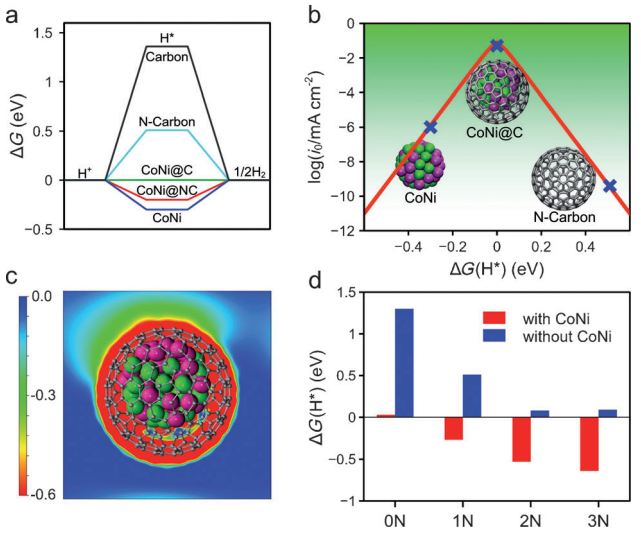

Figure 4. a) Gibbs free energy (ΔG) profile of the HER on various catalysts. b) Volcano plot of the polarized current (i_0) versus ΔG(H*) for a CoNi cluster, CoNi@C, and an N-doped graphene shell (N-carbon). c) The electronic potential of CoNi@C; the vacuum level was set to zero. d) The free energy of H adsorption (ΔG(H*)) on pure and N-doped (one, two, or three N atoms per shell) graphene shells with and without an enclosed CoNi cluster. Carbon gray, cobalt red, nickel green.

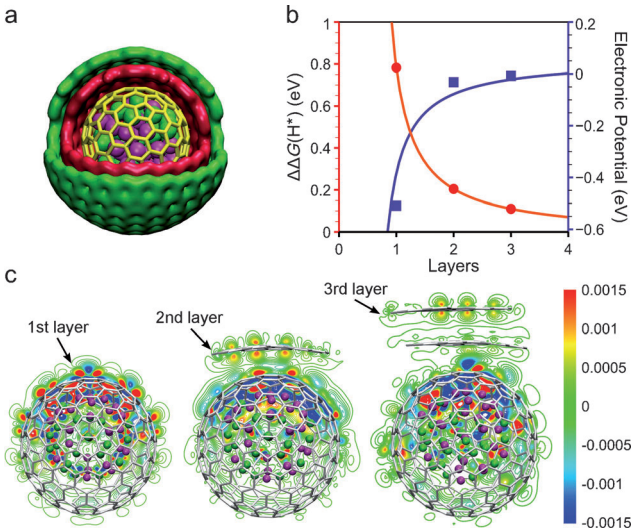

Figure 5. a) Schematic illustration of a CoNi alloy encapsulated in three-layer graphene. b) $\Delta\Delta G(H^*)$ (red line) and electronic potential (blue line) as a function of the number of graphene layers, where $\Delta\Delta G = \Delta G$ (without metal) $- \Delta G$ (with metal). c) Redistribution of the electron densities after the CoNi clusters have covered by one to three layers of graphene. The differential charge density ($\Delta\rho$) is defined as the difference in the electron density with and without the CoNi cluster. The red and blue regions are regions of increased and decreased electron density, respectively.

final product (Figure 4a). A good catalyst of the HER should have a moderate free energy for H adsorption (ΔG(H*)) to compromise the reaction barriers of the adsorption and desorption steps.[7,36] Thus, the dependence of ΔG(H*) on the measured current looks is represented by a volcano curve (Figure 4b). In our DFT calculations, the adsorption of H* on the CoNi alloy was found to be too strong whereas it was too weak on the N-doped graphene shell, resulting in low HER activity in both cases. In contrast, the ΔG(H*) value for the graphene shells of CoNi@C can be effectively tuned by the encapsulated CoNi alloy, resulting in a high HER activity (Figure 4a).

An analysis of the electronic potential of CoNi@C shows that the electronic potential on the side that is closer to the enclosed CoNi cluster is approximately 0.3 eV lower than that of the other sides, resulting in a higher proton affinity of the graphene shells (Figure 4c). Calculated electronic structures reveal that the stabilization of the H* species should originate from the increase in the electron density on the graphene shells near the CoNi cluster (Figure 5c), which can promote the HER activity. Furthermore, we also investigated how the nitrogen dopants cooperate with the metal clusters to promote the HER reaction. As shown in Figure 4d, increasing the number of nitrogen atoms from zero to three per shell leads to a decrease in $\Delta G(H^*)$ from 1.3 eV to 0.1 eV for graphene shells without an enclosed CoNi cluster, and the presence of the CoNi cluster leads to a further decrease in $\Delta G(H^*)$, which suggests that nitrogen dopants and enclosed metal clusters can synergistically promote the adsorption of hydrogen on graphene shells.

We further studied the effect of the graphene layer on the HER by using a model where one to three graphene layers encapsulate a CoNi cluster. The differential electron densities ($\Delta\rho$) in Figure 5c clearly illustrate that the electron of a CoNi cluster can penetrate through three graphene layers. Furthermore, the differences in the free energy of H adsorption [$\Delta\Delta G$(H*)] for the different layers with and without a CoNi cluster were used to describe the effect of the CoNi cluster on the HER. As shown in Figure 5b, the metal cluster induces a change in $\Delta\Delta G(H^*)$ of 0.8 eV when covered by a single graphene layer, whereas the effect decreases with an increase in the number of layers, but for the cluster with three graphene layers, the change still amounts to approximately 0.1 eV. Simultaneously, the difference in the electronic potential rapidly decreases from approximately −0.5 to 0 eV when the number of graphene layer is increased from one to three. This result further indicates that the effect of the enclosed metal clusters on the graphene shells will decline when the graphene shell consists of more than three layers. These results demonstrate that the graphene layer thickness of the CoNi@C catalysts has a substantial influence on the HER activity, the thinner the graphene shells, the higher the catalytic activity.

In summary, we have reported a hierarchical architecture that consists of ultrathin graphene shells (only 1–3 layers) that encapsulate a uniform CoNi nanoalloy (CoNi@NC), which provides a well-defined model for elucidating the role of carbon-encapsulated metal catalysts in the HER from theoretical calculations to the real system. Electrochemical measurements showed that CoNi@NC displays the best HER activity among the carbon-based electrocatalysts tested in acidic medium to date. DFT calculations indicate that the superior HER performance originates from the

modulation of the electron density and the electronic potential distribution at the graphene surface by a penetrating electron from the CoNi core. Meanwhile, reducing the number of graphene layers and increasing the amount of the nitrogen dopant can significantly increase the electron density in the graphene shells, which further enhances the HER activity. These findings pave the way towards the development of high-performance, inexpensive HER electrocatalysts that can be used in acidic electrolytes as well as other energy-related catalysts.

Received: September 26, 2014
Revised: November 17, 2014
Published online: January 7, 2015

Keywords: electrocatalysis · graphene · non-precious metals · hydrogen evolution reaction · nanoparticles

[1] M. S. Dresselhaus, I. L. Thomas, *Nature* **2001**, *414*, 332.
[2] J. A. Turner, *Science* **1999**, *285*, 687.
[3] J. A. Turner, *Science* **2004**, *305*, 972.
[4] S. Schuldiner, *J. Electrochem. Soc.* **1959**, *106*, 891.
[5] B. E. Conway, B. V. Tilak, *Electrochim. Acta* **2002**, *47*, 3571.
[6] W. C. Sheng, H. A. Gasteiger, Y. Shao-Horn, *J. Electrochem. Soc.* **2010**, *157*, B1529.
[7] B. Hinnemann, P. G. Moses, J. Bonde, K. P. Jørgensen, J. H. Nielsen, S. Horch, I. Chorkendorff, J. K. Nørskov, *J. Am. Chem. Soc.* **2005**, *127*, 5308.
[8] T. F. Jaramillo, K. P. Jørgensen, J. Bonde, J. H. Nielsen, S. Horch, I. Chorkendorff, *Science* **2007**, *317*, 100.
[9] Y. G. Li, H. L. Wang, L. M. Xie, Y. Y. Liang, G. S. Hong, H. J. Dai, *J. Am. Chem. Soc.* **2011**, *133*, 7296.
[10] H. T. Wang, Z. Y. Lu, S. C. Xu, D. S. Kong, J. J. Cha, G. Y. Zheng, P. C. Hsu, K. Yan, D. Bradshaw, F. B. Prinz, Y. Cui, *Proc. Natl. Acad. Sci. USA* **2013**, *110*, 19701.
[11] J. F. Xie, H. Zhang, S. Li, R. X. Wang, X. Sun, M. Zhou, J. F. Zhou, X. W. Lou, Y. Xie, *Adv. Mater.* **2013**, *25*, 5807.
[12] J. Deng, W. T. Yuan, P. J. Ren, Y. Wang, D. H. Deng, Z. Zhang, X. H. Bao, *RSC Adv.* **2014**, *4*, 34733.
[13] H. Vrubel, X. L. Hu, *Angew. Chem. Int. Ed.* **2012**, *51*, 12703; *Angew. Chem.* **2012**, *124*, 12875.
[14] Z. C. Xing, Q. Liu, A. M. Asiri, X. P. Sun, *Adv. Mater.* **2014**, *26*, 5702.
[15] H. T. Wang, D. S. Kong, P. Johanes, J. J. Cha, G. Y. Zheng, K. Yan, N. A. Liu, Y. Cui, *Nano Lett.* **2013**, *13*, 3426.
[16] L. Cheng, W. J. Huang, Q. F. Gong, C. H. Liu, Z. Liu, Y. G. Li, H. J. Dai, *Angew. Chem. Int. Ed.* **2014**, *53*, 7860; *Angew. Chem.* **2014**, *126*, 7994.
[17] R. Solmaz, G. Kardas, *Electrochim. Acta* **2009**, *54*, 3726.
[18] M. Gong, W. Zhou, M. C. Tsai, J. G. Zhou, M. Y. Guan, M. C. Lin, B. Zhang, Y. F. Hu, D. Y. Wang, J. Yang, S. J. Pennycook, B. J. Hwang, H. J. Dai, *Nat. Commun.* **2014**, *5*, 4695.
[19] E. J. Popczun, C. G. Read, C. W. Roske, N. S. Lewis, R. E. Schaak, *Angew. Chem. Int. Ed.* **2014**, *53*, 5427; *Angew. Chem.* **2014**, *126*, 5531.
[20] V. Artero, M. Chavarot-Kerlidou, M. Fontecave, *Angew. Chem. Int. Ed.* **2011**, *50*, 7238; *Angew. Chem.* **2011**, *123*, 7376.
[21] P. W. Du, R. Eisenberg, *Energy Environ. Sci.* **2012**, *5*, 6012.
[22] R. Subbaraman, D. Tripkovic, K. C. Chang, D. Strmcnik, A. P. Paulikas, P. Hirunsit, M. Chan, J. Greeley, V. Stamenkovic, N. M. Markovic, *Nat. Mater.* **2012**, *11*, 550.
[23] D. H. Deng, L. Yu, X. Q. Chen, G. X. Wang, L. Jin, X. L. Pan, J. Deng, G. Q. Sun, X. H. Bao, *Angew. Chem. Int. Ed.* **2013**, *52*, 371; *Angew. Chem.* **2013**, *125*, 389.
[24] J. Deng, L. Yu, D. H. Deng, X. Q. Chen, F. Yang, X. H. Bao, *J. Mater. Chem. A* **2013**, *1*, 14868.
[25] Y. Hu, J. O. Jensen, W. Zhang, L. N. Cleemann, W. Xing, N. J. Bjerrum, Q. F. Li, *Angew. Chem. Int. Ed.* **2014**, *53*, 3675; *Angew. Chem.* **2014**, *126*, 3749.
[26] H. T. Chung, J. H. Won, P. Zelenay, *Nat. Commun.* **2013**, *4*, 1922.
[27] J. Deng, P. J. Ren, D. H. Deng, L. Yu, F. Yang, X. H. Bao, *Energy Environ. Sci.* **2014**, *7*, 1919.
[28] X. C. Zou, X. C. Huang, A. Goswami, R. Silva, B. R. Sathe, E. Mikmekova, T. Asefa, *Angew. Chem. Int. Ed.* **2014**, *53*, 4372; *Angew. Chem.* **2014**, *126*, 4461.
[29] X. J. Zheng, J. Deng, N. Wang, D. H. Deng, W. H. Zhang, X. H. Bao, C. Li, *Angew. Chem. Int. Ed.* **2014**, *53*, 7023; *Angew. Chem.* **2014**, *126*, 7143.
[30] T. Fu, M. Wang, W. M. Cai, Y. M. Cui, F. Gao, L. M. Peng, W. Chen, W. P. Ding, *ACS Catal.* **2014**, *4*, 2536.
[31] C. Wang, P. Zhai, Z. C. Zhang, Y. Zhou, J. Ju, Z. J. Shi, D. Ma, P. S. Han, F. Q. Huang, *Part. Part. Syst. Charact.* **2014**, DOI: 10.1002/ppsc.201400039.
[32] F. Guinea, *Phys. Rev. B* **2007**, *75*, 235433.
[33] H. A. Chen, C. L. Hsin, Y. T. Huang, M. L. Tang, S. Dhuey, S. Cabrini, W. W. Wu, S. R. Leone, *J. Phys. Chem. C* **2013**, *117*, 22211.
[34] Y. J. Gao, G. Hu, J. Zhong, Z. J. Shi, Y. S. Zhu, D. S. Su, J. G. Wang, X. H. Bao, D. Ma, *Angew. Chem. Int. Ed.* **2013**, *52*, 2109; *Angew. Chem.* **2013**, *125*, 2163.
[35] N. Pentland, J. O. Bockris, E. Sheldon, *J. Electrochem. Soc.* **1957**, *104*, 182.
[36] J. K. Nørskov, T. Bligaard, A. Logadottir, J. R. Kitchin, J. G. Chen, S. Pandelov, J. K. Nørskov, *J. Electrochem. Soc.* **2005**, *152*, J23.

